Measurement by x-ray diffraction methods of the layer compressional elastic constant B in the lyotropic smectic-A (L_α) phase of the lecithin-water system

Daniel C. Wack* and Watt W. Webb
School of Applied and Engineering Physics, Cornell University, Ithaca, New York 14853-2501
(Received 4 January 1989)

A high-resolution synchrotron x-ray study of oriented, supported, hydrated dilauryl phosphatidylcholine in the lyotropic L_α (smectic-A or "fluid") phase shows that thermal fluctuations give rise to algebraic decay of positional order in stacking of the bimolecular lamellae, the so-called "Landau-Peierls" state. For planar monocrystalline samples of thickness 10–20 μm, the exponents derived from intensity profiles are in accord with harmonic theory. When combined with previous measurements of the splay elastic constant K in this lyotropic system, the exponents indicate a bulk compressional elastic constant $B=(1.9\pm1.0)\times10^8$ erg/cm^3, consistent in magnitude with values measured in thermotropic liquid crystals. Samples of thickness ~1–2 μm show anomalous behavior in the wings of the longitudinal intensity profiles, but are not in accord with harmonic theory, suggesting that surface effects partially quench the thermal fluctuations. Grandjean terraces on sample surfaces produce striking refractive effects at low Bragg angles.

I. INTRODUCTION

Lameller phases of lyotropic liquid crystals, in which roughly parallel lamellae or membranes are separated by a fluid medium, have attracted considerable theoretical[1,2] and experimental[3–6] attention recently because of the profound influence of thermal fluctuations on both the shape of individual membranes and the interactions between membranes. Examples of these phases can be found in hydrated phospholipids, where lipid bilayers alternate with water layers, and in ternary systems of surfactants, water, and oil, where surfactant monolayers separate layers of oil and water.

The first question to be addressed is how do thermal fluctuations disrupt the planar configuration of an isolated membrane? In the absence of surface tension or external constraints, Helfrich postulated[7] that the shape of an isolated membrane is governed by the free-energy functional

$$H_0\{u\}=\int d\mathbf{r}\,\tfrac{1}{2}\kappa_0(\nabla^2 u)^2 , \tag{1}$$

where $u=u(\mathbf{r})$ measures the displacement of the membrane from a planar configuration and κ_0 (in ergs) is the membrane *rigidity* constant. Theories based on (1) have been used to interpret the shape fluctuations of single-layer phospholipid vesicles[8] and red blood cells.[9] de Gennes and Taupin[10] investigated the role of curvature energy in a thermodynamic model of a bicontinuous microemulsion. They noted that the domains of oil and water separated by a surfactant monolayer compose a lattice whose lattice constant is roughly equal to the *coherence length* $\xi_\kappa\equiv a\exp(4\pi\kappa_0/3k_BT)$, where a is a molecular distance comparable to the in-plane spacing of two surfactant molecules. ξ_κ is the length scale over which a membrane maintains its orientational coherence until it is disrupted by thermal fluctuations. Helfrich[11] has suggested that these fluctuations should lead to an *effective rigidity* κ which is less than the bare value κ_0. Peliti and Leibler,[1] computing to one-loop order the renormalization-group equations which describe the renormalization of κ, confirmed that it is indeed easier to bend a membrane which is already slightly crumpled. Thus, they find that the rigidity depends explicitly on the linear size L of a 2D membrane,

$$\kappa(L)=\kappa_0[1-\tau\ln(L/a)] , \tag{2}$$

where $\tau=3k_BT/4\pi\kappa_0$. Safran *et al.*[12] have pointed out that renormalization of κ may play an important role in the phase stability of middle phase microemulsions.

The next theoretical issue concerns how thermal fluctuations disrupt a planar multimembrane system. The equilibrium thickness $\bar{l}$ of intercalated solvent in a multimembrane system results from the balance of molecular interactions and external constraints. When $\bar{l}$ is small, a stack of fluid membranes is equivalent to the smectic-A (Sm-A) phase of thermotropic liquid crystals. Traditionally, the effect of thermal fluctuations in this structure has been treated in the continuum limit by introducing a coarse-grained displacement variable $u(x,z)$, which depends on the stacking axis variable z in a continuous way. Symmetry arguments[13] then yield an effective Gaussian model for the free-energy density,

$$H_G=\int d^2x\,dz\left[\frac{1}{2}B\left[\frac{\partial u}{\partial z}\right]^2+\frac{1}{2}K(\nabla_\perp^2 u)^2\right]\Big/k_BT , \tag{3}$$

where B and $K\equiv\kappa_0/\bar{l}$ are the bulk moduli for layer compression (in erg/cm^3) and layer curvature (in erg/cm), and $\nabla_\perp^2$ denotes the Laplacian operator acting on in-plane coordinates (parallel to the local membrane surface). Within this harmonic model of the "1D" solid, thermal fluctuations prevent strict long-range order,[14] (LRO) but result in *quasi-long-range* translational order. Within this so-called *Landau-Peierls* system, the mean-

square displacement of a single layer, calculated by using the equipartition theorem and summing over the compressional and undulational acoustic modes, diverges logarithmically with system size L,

$$\langle u^2(\mathbf{r})\rangle \simeq \frac{k_B T}{2\pi\sqrt{KB}} \ln(L/\bar{l}) \ . \tag{4}$$

However, since these long-wavelength motions do not affect the short-range interlayer correlations, large parts of the system move almost in unison, and correlation functions decay weakly.[15] Caillé[16] showed that the displacement correlation function exhibits an anisotropic power-law decay with distance,

$$G_q(\mathbf{r}) = \langle \exp\{iq[u(\mathbf{r})-u(0)]\}\rangle \propto \begin{cases} (a^2/\lambda z)^x, & \rho \ll \sqrt{\lambda z} \\ (2a/\rho)^{2x}, & \rho \gg \sqrt{\lambda z} \end{cases} \tag{5}$$

where a is again an intermolecular distance, ρ denotes an in-plane distance, and the characteristic length $\lambda \equiv \sqrt{K/B} \sim d$. Importantly, the exponent x shows a quadratic scaling with wave vector,

$$x \equiv q^2 kT/8\pi\sqrt{KB} \ . \tag{6}$$

The peculiar asymptotic behavior of $G_q(\mathbf{r})$ leads to anisotropic singularities in the x-ray structure factor $S(\mathbf{q})$ about the harmonics $|\mathbf{q}_n| = n2\pi/d$,

$$S(\mathbf{q}) \propto \begin{cases} 1/(q_z - q_n)^{2-x}, & q_\perp \equiv 0 \\ 1/q_\perp^{4-2x}, & q_z \equiv 0 \end{cases} \tag{7}$$

where $\mathbf{q}$ is decomposed into components parallel (q_z) and perpendicular ($q_\perp$) to q_n. The elegant x-ray scattering experiments of Als-Nielsen *et al.*[17] found that the wings of the first quasi-Bragg peak in the Sm-A phase of the thermotropic liquid crystal 4-cyano-4-(n-octyloxy) biphenyl (8OCB) were indeed consistent with this power-law singularity form, and that measured values for x near the smectic-A–nematic transition agreed with values calculated using the harmonic approximation and independently measured values of the compressibility and splay elastic constants. Caillé's results for the scattering of x-rays by a Sm-A liquid crystal were extended by Gunther *et al.*[18] to include finite-size effects and the long-range order induced by an external magnetic field. As has also been noted for the finite 2D harmonic lattice,[19] the structure factor retains the infinite system form far from the Bragg point, but is rounded off by a Gaussian peak whose width is of order L^{-1}.

The low degree of short-range order in thermotropic Sm-A liquid crystals leads to a near sinusoidal mass-density wave, so that no significant scattered x-ray intensity appears in harmonics greater than the first. In contrast, lyotropic smectic liquid crystals, in which hydrophobic effects drive a higher degree of local order normal to layers of surfactant aggregates, often display a number of harmonics limited only by the available intensity and recording time. This feature has been used to great advantage in swelling experiments to map the lipid bilayer structure factor, and through Fourier synthesis, construct the projected electron density.[20]

When the thickness of intercalated solvent is comparable to the membrane thickness, thermally activated curvature fluctuations of individual membranes become significant contributors to intermembrane interactions. Recently attention has focused on the microscopic description of interacting, fluctuating membranes, to elucidate the interplay between molecular and *steric* interactions. Because the average distance $\bar{l}$ between membranes can often be varied by the addition of solvent, the lamellar phases of lyotropic liquid crystals offer a unique experimental system for a systematic study of this interplay. Helfrich[21] has noted the possibility of a long-ranged, repulsive mechanism, whose origin lies in the mutual steric hindrance of thermally undulating membranes, which can compete with, and possibly defeat, long-range attractive van der Waals interactions. He suggested that the loss of entropy due to the interactions of fluctuating membranes should lead to an *effective contribution* to the free energy of the form

$$V_s(\bar{l}) \sim \frac{(k_B T)^2}{\kappa \bar{l}^2} \ . \tag{8}$$

Steric repulsions have also arisen in the context of fluctuating domain walls in the stripe-domain phase of the 2D solid,[22,23] steps on a crystal surface,[24] and 2D polymer systems.[25] Lipowsky and Leibler[2] have shown that the process of swelling a lamellar phase by addition of solvent, which leads to a strong increase of the mean separation, can be viewed as a phase transition, which they termed *complete unbinding*. They also showed that the system exhibits quasi-long-range translational order. Larche *et al.*[3] have prepared extremely dilute lyotropic smectic samples, in which ~4-nm ionic surfactant bilayers were separated by ~650 nm of oil, and found that the angular distribution of scattered light (at optical wavelengths) showed two sharp (quasi-) Bragg peaks. They attributed this apparent LRO to stabilization by steric repulsion. Safinya and co-workers,[4,6] in synchrotron x-ray studies of swollen lamellar phases of a quaternary microemulsion system, found evidence of a variation with membrane spacing of the exponent $x(\bar{l})$ (which describes algebraic decay) consistent with the predicted effects of entropic steric repulsion.

Previous work on determining the magnitude of the rigidity constant κ has focused on free-floating unilamellar phospholipid vesicles, and, in multicomponent systems, on the lamellar microemulsion phases. By measuring the time correlation function for fluctuation amplitudes of the lowest normal modes, Schneider *et al.*[8] found $\kappa \sim 1-2\times10^{-12}$ ergs for both spherical and cylindrical vesicles of dimyristoyl phosphatidylcholine (DMPC). Servuss *et al.*[26] also found $\kappa \sim 2\times10^{-12}$ ergs by measuring the mean-square amplitude of the bending mode of long unilamellar cylindrical vesicles. The rigidity for lamellar microemulsion phases appears to be much lower than in the phospholipid systems. Di Meglio *et al.*[27] found $\kappa \sim (2-6)\times10^{-15}$ ergs both by the local technique of spin labelling, and by quasielastic light scattering from bulk undulational modes of a lamellar microemulsion phase.

There is considerably less known about the magnitude

of the layer compressibility modulus B, in lyotropic lamellar systems. B can be obtained through the techniques of Brillouin light scattering, ultrasonic wave propagation, or forced Rayleigh scattering. In thermotropic smectics, there is a fairly large scatter in the values of B obtained by these techniques, those obtained at high frequencies ($\sim 10^9$ Hz) being a factor of 10–20 greater than those at low frequencies ($\sim 10^3$ Hz). As noted by Prost,[28] the high-frequency techniques are beyond the hydrodynamic regime (set by the characteristic time for molecular relaxations, typically 10^{-7} sec), while the low-frequency measurements of B may be influenced by generation and motion of dislocations. Using Brillouin light scattering, LePesant *et al.*[29] found that for the Sm-A phase of dipalmitoyl phosphatidylcholine (DPPC) at 35% water (by weight) $B \leq 5\times 10^9$ (erg/cm^3); i.e., below the limits of detection for their experiment. Using the interdigitated electrode technique, Marcerou *et al.*[30] were able to measure the second sound mode on an L_α phase DPPC sample at 4% water and $T=115$°C, and found $B \simeq 1.6\times 10^9$. Although they also studied a DPPC sample at 25% water and $T=47$°C [which is much closer to the hydration condition of our dilauryl phosphatidylcholine (DLPC) samples], they did not report a value of B for this sample. Safinya *et al.*[4] found $B=6\times 10^7$ erg/cm^3 for powder samples of the concentrated lamellar phases formed by the quaternary mixture sodium dodecyl sulfate (SDS)–water–pentanol– dodecane. Smith *et al.*,[5] in an x-ray study of freely suspended films of DMPC, found that the slopes of the higher harmonics were consistent with a value $B=2\times 10^{10}$ erg/cm^3; this measurement was potentially corrupted by inhomogeneities, however. The widths of longitudinal profiles in this sample increased systematically with harmonic, however, inconsistent with quasi-long-ranged-order (QLRO) or finite-size effects,[31] but consistent with inhomogeneities resulting from nonequilibrium water concentrations or radiation-damage effects. We have observed inhomogeities due to nonequilibrium of water chemical potential, and below we discuss their relaxation.

There have been few direct probes of spatial fluctuation phenomena displaying algebraic decay. Through the use of channel-cut Si(220) monochromator and analyzer crystals, Als-Nielson *et al.*[17] illustrated the importance of steep instrumental function wings in measurements of power-law singularities. Moncton and Pindak[32] found evidence of algebraic wings in the first harmonic of a four-layer freely suspended smectic-B liquid crystal, a model 2D solid system. Power-law behavior was also observed by Huang *et al.*[33] in the first harmonic of a monolayer of Xe on the basal planes of graphite. Synchrotron x-ray scattering measurements by Mochrie *et al.*[23] demonstrated power-law behavior at five harmonics of the mass density wave in the weakly incommensurate stripe-domain phase of stage-4 bromine-intercalated graphite, and confirmed the scaling of exponents with q^2 expected within the harmonic approximation to the 2D solid.

In this paper we report a high-resolution synchrotron x-ray scattering study of the layer-spacing fluctuations in room-temperature, hydrated dilauryl phosphatidylcholine (DLPC) aligned multilamellar samples supported on a solid substrate. Since under these conditions each DLPC bilayer is a fluid membrane, the samples are lyotropic Sm-A liquid crystals, also known as the $L\alpha$ phase, which as we have discussed above, should display an algebraic decay of positional correlations. Our intent was to probe the extent to which stacking fluctuations disrupt long-range translational order of the 1D Sm-A lattice, by studying in detail the quasi-Bragg-diffraction profiles. By directly measuring the exponent x in reciprocal-space scattering profiles, we show the presence of QLRO in thick samples, and find that the fluctuations are quenched in thinner samples. Assuming values for κ from independent measurements, we can then deduce values for the compressional elastic constant B in these hydrated phospholipids.

II. EXPERIMENTAL METHODS

A. X-ray optics

The scattered intensity $I(\mathbf{q})$ at scattering vector $\mathbf{q}$ results from a convolution of the sample structure factor $S(\mathbf{q})$ with the instrumental resolution function $R(\mathbf{q})$. Since the signature of quasi-long-range order is the presence of anomolously intense "wings," an attempt to probe this state must employ a well-characterized instrumental resolution function, else the contribution of the sample structure factor is liable to be confused with that of the scattering instrument, an error that befell some earlier investigators.[34] Since $S(\mathbf{q})$ possesses no intrinsic width (aside from finite-size-induced contributions), but a characteristic slope, the instrument function should approximate a δ function as closely as possible. It should have a narrow width, and more importantly, steep wings. X-ray optics can obtain these qualities through the use of multiple Bragg reflections in channel-cut perfect single crystals of silicon, as first demonstrated by Bonse and Hart.[35]

A schematic diagram of the optical arrangement which we employed on the A3 line at Cornell High Energy Synchrotron Source (CHESS) in Ithaca, New York, is shown in Fig. 1. The x-ray source point was 10 m upstream of the monochromator, which consisted of a pair of Si(111) single crystals whose faces were maintained parallel to select a twice reflected beam of energy 8.041 keV from the white beam incident on the first crystal. Although at the time of our runs this monochromator possessed sagittal focusing capability because of a slotted second crystal, we found that as the second crystal was bent, an unacceptable distortion of the direct beam profile developed. Thus we operated the monochromator without focusing. The stability of the monochromator tuning proved to be troublesome at the beginning of a storage ring fill, and during those runs when the wings of a wiggler beam spilled over the optics of an adjacent line and struck the edge of the A3 first crystal.

After exiting an He flow tube at the front of the hutch, the beam was collimated by slits S_1 in both horizontal and vertical planes. Since a large d-spacing sample (typi-

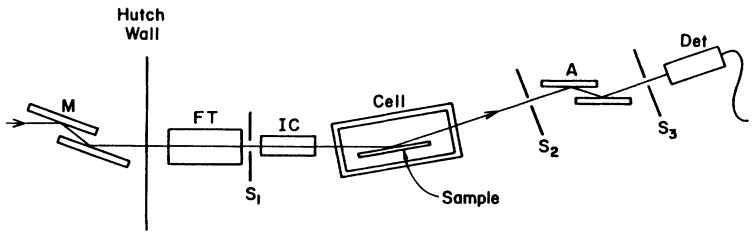

FIG. 1. Schematic diagram in the scattering (vertical) plane of the x-ray optics used on the A3 line at CHESS. Monochromator M and analyzer A were Si(111) single crystals; FT, helium flow tube; S_1, collimating slit; IC, monitor N_2 ion chamber; S_2 and S_3, guard slits; detector Det was either a scintillator or an argon-ion chamber.

cally 4.5 nm) was being observed in reflection (Bragg angle of first reflection $\sim 1°$) from a sample whose length was roughly 2 cm, the beam height had to be limited to illuminate the sample alone to minimize parasitic scatter at low harmonics. Thus at each harmonic, while keeping the sample and analyzer tuned to the peak, the vertical aperture of S_1 was reduced until the diffracted intensity began to dip. The collimated beam was then monitored by a transmission N_2-ion chamber, which provided the normalization signal necessary for a step scan under conditions of decaying and drifting direct-beam intensity. Next, the beam struck the oriented lipid sample supported on a 1-in. polished Si(111) wafer substrate enclosed in a controlled humidity cell. This cell was mounted on a Huber 410 rotation stage such that the rotation axis lay in the plane of the wafer surface. A second Huber 410, concentric with the first, was used to control the scattered-beam analyzer which was fixed to the "two-θ" arm. This angular analyzer was a double-reflection channel-cut Si(111) single crystal, cut for use near 9 keV.[36] The 1-cm horizontal width of slit S_2 25 cm from the sample defined the scattering resolution in the horizontal plane, while its vertical aperture was reduced until the direct beam was clipped, to prevent stray radiation from entering the analyzer in the vertical plane. To further reduce collection of stray scattering, slit S_3 limited the acceptance of the aperture of the Bicron scintillator detector to those rays leaving the analyzer crystal. For measurement of the direct-beam properties the scintillator was replaced by an argon-ion chamber.

B. Characterization of resolution function

The important components of the instrumental resolution function were directly measured to insure that their contributions to the scattering profiles were negligible. The *longitudinal* component (parallel to the scattering vector) is determined by the convolution of the *nondispersive* profile, which arises from the dynamical scattering properties of the monochromator and analyzer single crystals, with the *dispersive* profile, which reflects the spectral distribution of radiation produced by the monochromator. Each of these profiles can be directly measured. The nondispersive profile was measured by scanning the analyzer crystal, with orientation as shown in Fig. 1, through the direct beam, with the analyzed rays being recorded with an argon-ion chamber. The result is shown in Fig. 2, which plots on both linear and logarithmic scales the intensity versus analyzer misset angle. A solid line representing a Gaussian function of equivalent full width at half maximum (FWHM) is also shown to indicate the degree to which the measured profile departs from the paradigmatic functional form. The theoretical width $\delta\theta_D$ of the reflectivity curve ("Darwin width") for Si(111) at 8 keV is 0.0019°, and after convolution with itself one expects to see 0.0027°. Since the measured profile shows a FWHM of 0.0023°, we find that the double-reflection process has reduced the width by only 15%. The asymmetry in the wings of the nondispersive profile seemed to be intrinsic to the analyzer crystal, as it was not perturbed by adjustments to the analyzer-crystal orientation with respect to the monochromator, or even a complete change of the monochromator second crystal.

The dispersive profile was measured by putting the analyzer crystal into a dispersive orientation with respect

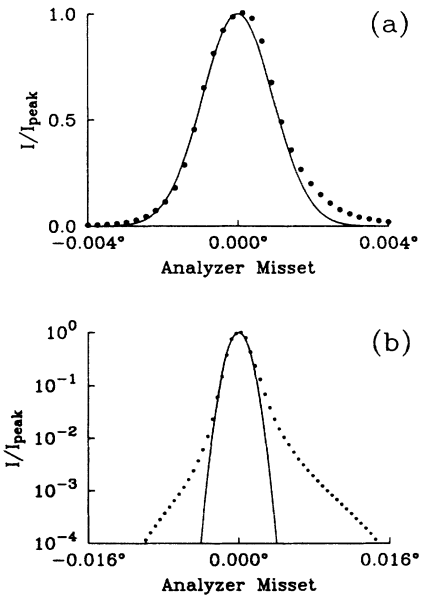

FIG. 2. Scan of the direct beam by a Si(111) double-reflection channel-cut analyzer crystal in the nondispersive orientation (closed circles) and a Gaussian of the same FWHM (solid line): (a) normalized intensity on a linear scale, (b) normalized intensity on a log scale.

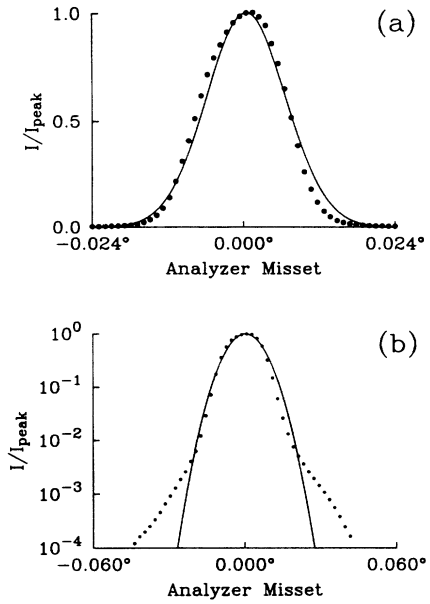

FIG. 3. Scan of the direct beam by a Si(111) analyzer crystal in the dispersive orientation (closed circles) and a Gaussian of the same FWHM (solid line): (a) normalized intensity on a linear scale, (b) normalized intensity on a log scale.

to the monochromator (i.e., flipping by 180° the orientation shown in Fig. 1), and again scanning through the direct beam. The measured profile, shown in Fig. 3, displays a FWHM of 0.015°. This property of the monochromated beam can be understood as follows. The parallel crystals of the monochromator pass the full vertical divergence $\delta\theta_v$ of the incident beam, which depends on the electron and photon energies and here is $\simeq 0.0082°$,[37] giving a bandpass of $\delta\lambda/\lambda = \delta\theta_v / \tan(\theta_{111}) \simeq 5.6\times 10^{-4}$, where $\theta_{111} = 14.3°$ is the Bragg angle for Si(111) at 8 keV. Since the dispersive characteristics of the analyzer are matched to the monochromator, the angular range $\delta\theta_A$ through which the analyzer travels to scan the direct beam is $2\delta\theta_v \simeq 0.0164°$, which compares well with the measured FWHM. (At a more sophisticated level, the vertical divergence is the result of a convolution of the angular profile of the synchrotron radiation emitted by a single electron with the statistical distribution of electron trajectories within the storage ring.) The measured dispersive profile actually involves a convolution with the nondispersive profile as well, but since $\delta\theta_A \gg \delta\theta_D$, the nondispersive component can be neglected in the measurement. To obtain the angular distribution of the dispersive component at *sample* Bragg angles θ_S, the abscissas of the measured profiles must be scaled by the factor $\tan\theta_S/\tan\theta_{111}$.[t] The complete longitudinal profile of the instrument function at a given sample Bragg angle is then obtained by convolving the nondispersive profile with the scaled dispersive profile.

The transverse component of the instrument function (which lies in the scattering plane, but perpendicular to the scattering vector) is determined by the distribution of domain orientations in the sample, or *mosaic spread,* as this is usually much greater than the acceptance of the analyzer crystal. In our experiment, a measurement of mosaic spread required demounting the analyzer crystal, because space constraints in the hutch prevented insertion of an ion chamber prior to the analyzer. Alignment of the analyzer proved so time consuming that, after the direct beam profiles had been characterized, we could not afford to remove the analyzer crystal during the limited beam time available. Thus it was not possible to measure directly the sample mosaic spreads. Finally, the component perpendicular to the scattering plane is determined by the slits defining the horizontal apertures in the optical system, which in our case resulted in a triangular profile with a FWHM of 40 mrad.

Some additional aspects of the measurement are worth mentioning. We found a significant reduction (by a factor of 2–5) in scattered background levels when the monochromator was detuned by 50%. Detuning drastically reduces the transmission of odd harmonics of the 8-keV beam through the Si(111) monochromator. The remaining background was largely due to scattering from air in the illuminated volume above the sample. Counting rates in the lower harmonics were above the linear regime for a scintillator but below the sensitivity of an argon-ion chamber. To keep the scintillator from saturating, Al-foil absorbers were inserted in the direct beam until the flux at the peak was less than 2×10^5 photons/sec. At these data rates, under single-photon counting conditions, the counting loss due to photon bunching is nontrivial, so the appropriate correction was applied.[38] The time scale for scanning a single harmonic, and thus the counting statistics in the wings, was limited by the drift in the first crystal of the monochromator (0.0001–0.001 °/min). Thus the total scan through a harmonic was accomplished before the monochromator had drifted very far from the 50% detuned condition.

C. Sample preparation

Supported, hydrated lipid samples of $\sim(2\text{cm})^2$ were prepared by evaporation from organic solvent onto a polished, single crystal Si(111) wafer. The wafer was first soaked in a 0.2% solution of octadecyltrichlorosilane in a solvent mixture hexadecane:carbon tetrachloride:chloroform (80:12:8) for 1 day to obtain a hydrophobic surface. Then $\sim 20\mu$l of DLPC in ethanol (200 mg/ml) was deposited onto the substrate. DLPC was chosen because at room temperature the hydrated lipid is deep in the Sm-A phase, where the lattice constant has a much smaller temperature coefficient than if one worked closer to the "main" or chain melting phase transition. Thus we could afford to use an unthermostated sample cell. When the amount of solvent deposited was such that the solvent had mostly evaporated right at the point at which the drop reached its spreading limit, the resulting lipid deposit had a favorable uniformity of thickness. If more than this was deposited, the solution tended to contract into islands after reaching the spreading limits, leaving a very clumped distribution of lipid. The combination of ethanol and a hydrophobic surface gave good drop-spreading properties. But successful deposition required

moderate room relative humidities to prevent the lipid from crystallizing, which destroyed the alignment of the sample. From the amount of lipid deposited and the areas covered, the average thickness for our samples was $\sim 10\mu$m, although data will also be presented for $\sim 1-2\mu$m samples, which were obtained when samples were prepared under low-humidity conditions at CHESS. After the solvent was allowed to evaporate completely, samples were placed in a closed cell, whose schematic is shown in Fig. 4, which incorporated a reservoir for a saturated salt solution to control the relative humidity of the vapor phase above the sample, and thus the chemical potential of water within the lipid multilayer. Equilibration of samples often involved hours; we will discuss below our observations of inhomogeneities resulting from nonequilibrium states of water concentration.

III. RESULTS

We probed longitudinal profiles 3–4 decades below the peak intensity; slight inhomogeneities in either lipid composition or water concentration became apparent as distortions of the intensity distribution. Since this kind of sensitivity had not been previously achieved, problems due to inhomogeneity have not been appreciated. For instance, Franks and Lieb[39] found that as far as measurement of integrated intensities were concerned, equilibration times of an oriented, supported lipid sample after a change in the humidity of the vapor phase above the sample were on the order of 10 min to 1 h. We also found that most of the diffracted intensity appears at the new angular position on the time scale of tens of minutes, but that at the level of 10^{-1} to 10^{-4} from the peak, a residue of intensity at the previous peak position decayed on the time scale of 10–20 h. The approach to hydration equilibrium could be monitored by executing longitudinal scans on harmonics 2, 4, and 6. Inhomogeneous samples displayed broadened or asymmetric line profiles, which evolved with time toward the resolution-limited line profile. Although there is some evidence of staging disorder in lipid multilayers,[40] which also produces distortions of line profiles, we did not observe such equilibrium states.

For example, we show in Fig. 5 longitudinal scans of the fourth harmonic of a DLPC sample at 8 and 20 h after a change in the relative humidity from 76% to 98%.

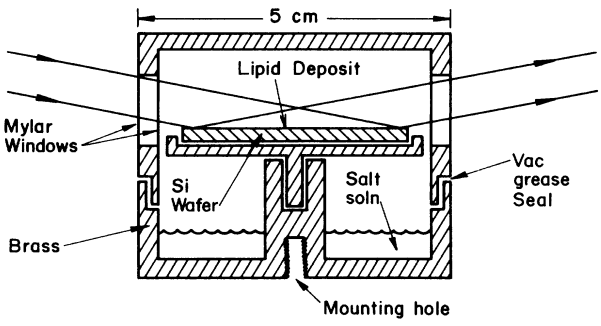

FIG. 4. Schematic diagram in the scattering (vertical) plane of the controlled humidity cell.

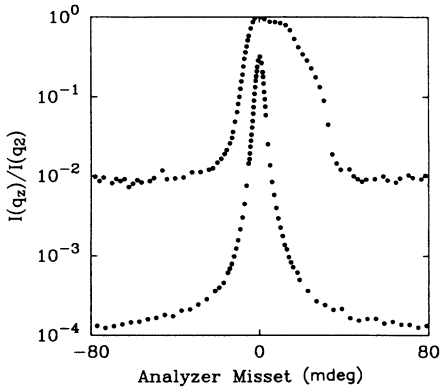

FIG. 5. Longitudinal scans of the fourth harmonic of DLPC ($T=28°$) at 8 hours (upper) and 20 hours (lower) after a change in relative humidity from 76% to 98%: $\log_{10}$ of normalized intensity vs analyzer angular offset. Curves displaced vertically for clarity.

In an attempt to reach greater hydration levels, we tried enclosing samples with Dextran solutions. In Fig. 6 we show longitudinal scans of the fourth harmonic of a DLPC sample at 6 and 26 h after a change in the relative humidity from 76% to approximately 99% (50 wt. % Dextran solution). When a 40 wt. % Dextran solution was used to control the relative humidity, a DLPC sample showed inhomogeneity in water concentration even after a wait of 33 h.

The presence of *Grandjean terraces*[13] in samples prepared by this technique has important consequences for longitudinal profiles. To illustrate the consequences of terracing, we show in Fig. 7 an example of the redistribution of diffracted intensity in longitudinal scans of low harmonics by refractive effects at the nonuniform sample surface. This sample, DLPC at 76% relative humidity and 28°, had a lattice constant of 4.44 nm. Viewed in reflection of room light, it showed vivid Fizeau fringes, indicating a thickness of 1–2 μm, as well as a faint tra-

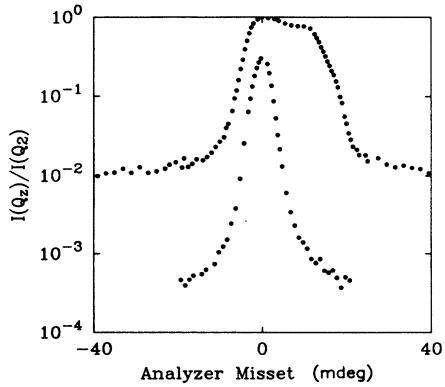

FIG. 6. Longitudinal scans of the fourth harmonic of DLPC ($T=28°$) at 6 h (upper) and 26 h (lower) after a change in relative humidity from 76% to approximately 99% (a 50 wt. % dextran solution): $\log_{10}$ of normalized intensity vs analyzer angular offset. Curves displaced vertically for clarity.

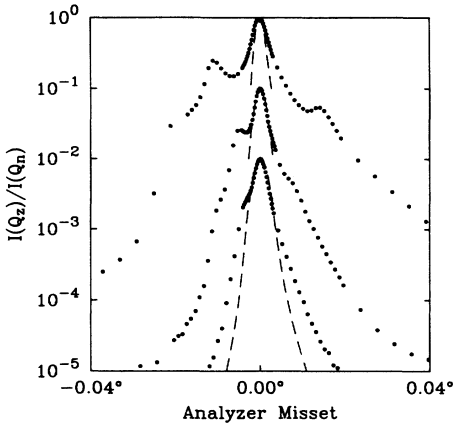

FIG. 7. Longitudinal intensity profiles of the first three harmonics of sample 4 (DLPC at $T=28°$ and $d=4.44$ nm): $\log_{10}$ of normalized intensity (closed circles) vs analyzer angular misset, together with the longitudinal resolution function at each harmonic (dashed lines). Successive harmonics displaced vertically by one decade for clarity, with the first on top.

cery of white lines arranged in the characteristic pattern of Grandjean terraces. The central peak of the longitudinal scans arises from rays which have entered and exited the sample through the terrace steps; i.e., surfaces parallel to the scattering planes of the lamellar liquid crystal. Entering each interface at a Bragg angle θ_B, these rays undergo a refractive deviation[41] $\Delta\theta_B=2\delta/\sin 2\theta_B$, where δ is the refractive index decrement. For lipid-water mixtures at $\lambda\simeq 0.15$ nm, $\delta\simeq 3.5\times 10^{-6}$. At the first harmonic $\theta_B\simeq 0.98°$ and the deviation amounts to 0.012°, roughly four times the longitudinal instrument resolution.

Rays which enter or exit the sample by a terrace *wall* (a surface perpendicular to the scattering planes) undergo negligible refractive deviation and thus diverge from the pure Bragg-diffracted beam, appearing at $-\delta\theta_B$ relative to the primary peak. Some rays both enter and exit the sample through a terrace wall, appearing at $-2\delta\theta_B$, while some rays penetrate a corner of the terrace before being diffracted, experiencing *excess* refractive deviation relative to the primary peak. Figure 7 also shows that the refractive deviations collapse into the core at successive harmonics, because of the increase in Bragg angle. By the fourth harmonic refractive effects are negligible, and the longitudinal profiles can be analyzed for the presence of QLRO. The scattered intensity decreases with harmonic due to the Lorentz factor and the increased penetration of the direct beam though the thin sample. Harmonics beyond the sixth harmonic did not have enough signal to noise in the wings for determination of exponents.

We present measurements of intensity profiles from four samples. As deduced from the amount and area of the lipid deposited, and the characteristics of the interference fringes exhibited in reflection of room light from the sample surfaces, two samples have thicknesses of approximately 10–20 μm, while the other two were in the range 1–2 μm. All samples which had reached hydration equilibration showed longitudinal peak widths identical to the instrument resolution; i.e., no finite-size effects were apparent in these samples at Si(111) resolution. No evidence of radiation damage appeared within the exposure times necessary to characterize both longitudinal and transverse profiles of the first six harmonics, approximately 4 h at an average incident intensity of 10^{10} photons/sec. At each harmonic, scans were extended until a flat and well-characterized background was obtained. In the data presented below, this background contribution has been subtracted, and the profiles have been normalized by the peak intensity. For longitudinal scans, the instrumental resolution is indicated by a dashed line to indicate both the resolution-limited nature of the peak widths as well as the degree to which these profiles depart from the resolution function in the wings.

We first present data for the thicker pair of samples. Sample 1, within a cell at 86% relative humidity and 28°, showed a lattice constant of 4.47 nm, while sample 2, at 98% relative humidity, showed a lattice constant of 4.78 nm. For both of these samples, the smooth distribution of intensity in longitudinal scans of the first two harmonics indicated a lack of significant terracing on the free surface. Figure 8 shows longitudinal scans of the fourth and sixth harmonics of sample 1, and indicates the exponent derived by fitting a linear function to the data after logarithmic scaling. The error was derived by finding the limits at which the value of χ^2 doubled. Assuming the scaling relation $x_n\propto q_n^2$ from harmonic theory, the measured exponents imply values of x_n at the first harmonic of 0.011 ± 0.005 (from the fourth) and 0.020 ± 0.005 (from the sixth). Thus within experimental error our results for the longitudinal exponent are consistent with the scaling relation of harmonic theory. If we further assume a value for the bulk splay elastic constant $K=3\times 10^6$ ergs/cm, based on the value of κ measured by Schneider *et al.*, we deduce a value for the bulk compressional elastic constant B of $(1.9\pm 1.0)\times 10^8$ ergs/cm^3. This value for B is comparable in magnitude to that measured in thermotropic liquid crystals, and represents the first measurement of the bulk compressional elastic constant in the Sm-A phase of the DLPC-water system.

In Fig. 9 we show a longitudinal profile for the fourth harmonic of sample 2 (the second of the thicker samples). The derived asymptotic slope of the line profile is -1.74 ± 0.13, which implies a value for x_n at the first harmonic of 0.016 ± 0.008. Within experimental error, this result is consistent with that obtained from the previous sample. Measurements on this sample of the longitudinal profile at the sixth harmonic did not possess sufficient counting statistics to permit analysis of the asymptotic slope.

Next we present data for the second and thinner pair of samples. Sample 3 was at 86% relative humidity, 28°, and had a lattice constant of 4.47 nm, while sample 4 was at 76% relative humidity, 28°, and had a lattice constant of 4.44 nm. (Samples held at relative humidities below 76% exhibited coexisting lamellar phases, with the longer period at 4.85 nm, undoubtedly indicating that the two-phase region $L_\alpha+L_{\beta'}$ has been entered.) Their optical

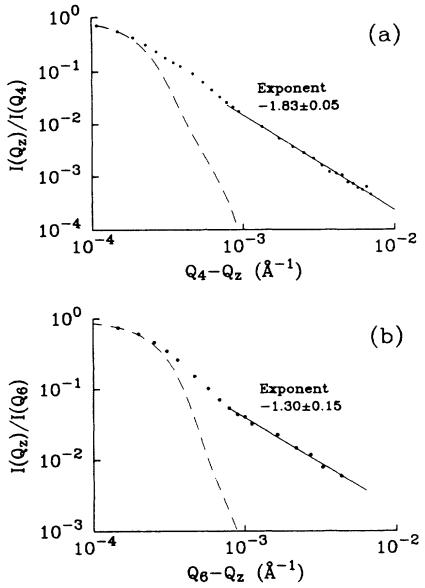

FIG. 8. Longitudinal scans of the fourth and sixth harmonics of sample 1 (DLPC at 28°, 86% relative humidity, $d=44.7$ nm): $\log_{10}$ of normalized intensity vs log of scattering vector distance from harmonic Q_n. Experimental data shows as solid points, measured longitudinal resolution function shown as dashed line, and a fit to the asymptotic slope is shown as a solid line. (a) fourth harmonic, (b) sixth harmonic.

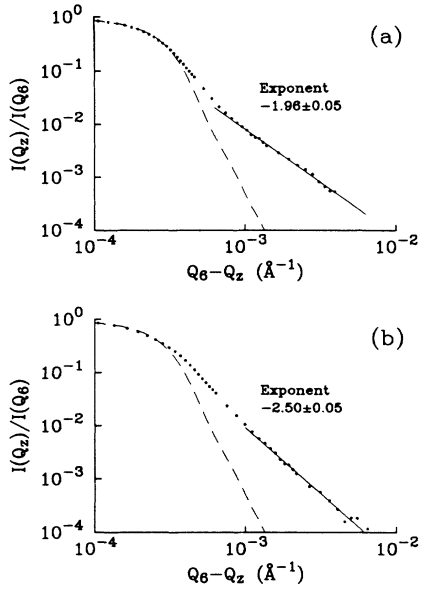

FIG. 10. Longitudinal scans of the sixth harmonic of samples 3 and 4: log of normalized intensity vs $\log_{10}$ of scattering vector distance from harmonic Q_6. Experimental data are shown as solid points, the instrument resolution as a dashed line, and a fit to the asymptotic slope as a solid line, with the resulting exponent indicated. (a) Sample 3: 86% relative humidity, 28°, $d=4.47$ nm. (b) Sample 4: 76% relative humidity, 28°, $d=4.44$ nm.

appearance showed no striations or point defects, only a faint tracery of white lines in a terracing pattern. Vivid and slowly varying Fizeau fringes indicated a thickness on the order of 1–2 μm. Both samples displayed evidence in the longitudinal scans of well-defined terracing on a significant portion of the illuminated surface, as discussed in the experimental section. Figure 10 shows longitudinal scans of the sixth harmonic of each sample, as well as the result of a fit to the asymptotic slopes. Both show line profiles which follow the instrument function, indicated by a dashed line, near the peak. Thus the samples are homogeneous, with no evidence of finite-size effects. Far from the peak, the experimental data extend significantly above the longitudinal resolution function. Thus it appears that thermal fluctuations in the lamellar spacing have disrupted true long-range order. However, the exponents yielded by these samples are greater in magnitude than that measured for sample 1. Sample 3, since it shows a slope -1.96 ± 0.05, could still be construed as consistent with the predictions of harmonic theory [Eq. (7)], but the value of B which this exponent implies is a factor of 40 greater than that deduced from sample 1. The slope shown by sample 4 is significantly greater than 2, however, in contradiction to the results of harmonic theory. Since there are no indications of experimental artifacts in the thinner set of samples, and since the two sets of samples differ significantly only in their thicknesses, our results seem to indicate that in the $\sim$1-μm samples, boundary effects have altered the thermal fluctuation spectrum expected for an infinite sample. de Gennes[13] has pointed out that static surface distortions can propagate long distances into the bulk of Sm-A samples before relaxing. One expects that a zero surface displacement boundary condition has similarly long-ranged effects. To our knowledge, a theory which rigorously accounts for boundary effects on the thermal fluctuation spectrum of the Sm-A phase is not available. If our interpretation is correct, it is perhaps surprising that the *par-*

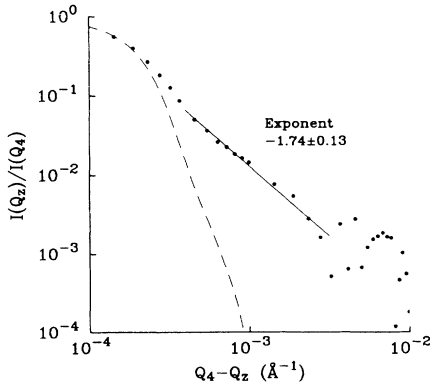

FIG. 9. Longitudinal scan of the fourth harmonic of sample 2 (DLPC at 28°, 98% relative humidity, $d=47.8$ nm): $\log_{10}$ of normalized intensity vs $\log_{10}$ of scattering vector distance from harmonic Q_n. Experimental data shown as solid points, measured longitudinal resolution function shown as dashed line, and a fit to the asymptotic slope is shown as a solid line.

tially quenched samples maintain an algebraic appearance, and it would be significant that the crossover between bulk and quenched appearance of the x-ray profiles occurs in the 1–10 μm regime. Data at greater scattering vector displacements from each harmonic, and at higher harmonics, would be helpful in discriminating surface effects, but would require a much brighter x-ray source.

Finally, we will discuss our measurements of *transverse* intensity profiles for these samples. As mentioned in Sec. II, obtaining transverse profiles, by performing a θ scan with fixed $Q_z = Q_n$, was simple, but calibrating the mosaic spread, which is required to interpret fully the transverse profiles, unfortunately could not be achieved. Qualitative analysis of the measurements however reveals some systematic and interesting behavior. Figure 11 shows representative transverse profiles at $Q_z = Q_n$ for a series of harmonics of samples 2 and 3. Regarding the asymptotic slopes of these profiles, neither sample shows any significant change with harmonic. Sample 2 shows exponents of -1.5 ± 0.2, while sample 3 shows exponents of -2.5 ± 0.2. It seems reasonable to presume that these wings are dominated by the wings of the sample mosaic distribution. What does change with harmonic, and systematically so for all samples, is exemplified by the data in Fig. 12, which shows on a linear scale the transverse scans for harmonics $n = 1$, 2, 3, 4, and 6 of sample 3. The observed increase in angular width of the transverse scans is surprising if one assumes that the central region of such scans should be dominated by the mosaic distribution, which, apart from penetration depth effects, is constant for a series of harmonics of the Sm-A lattice. But bearing in mind that the observed profile results from a convolution of the mosaic distribution with, for bulk samples, the anisotropic singularities of Eq. (7), or, for finite and partially quenched samples, a potentially more complex structure factor, the interpretation of this increase in angular width is not straightforward. To progress any further in understanding the transverse scans requires measurements of the mosaic distributions and an explicit expression for the structure factor of a partially quenched sample.

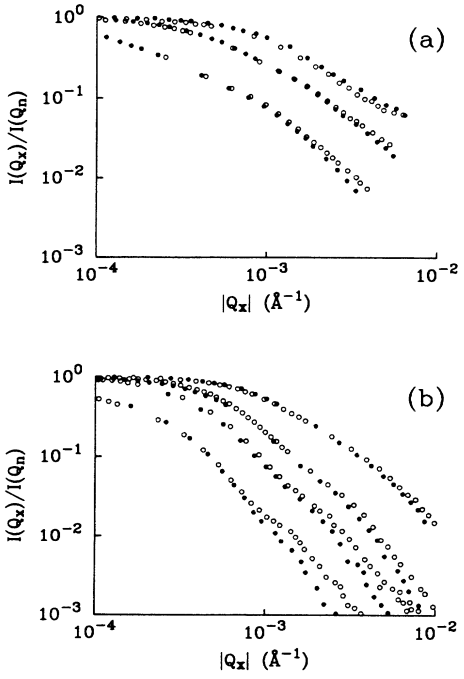

FIG. 11. Transverse intensity profiles at $Q_z = Q_n$ for a series of harmonics: $\log_{10}$ of normalized intensity vs $\log_{10}$ of transverse component of scattering vector. (a) sample 2, harmonics 2, 3, and 4; (b) sample 3, harmonics 2, 3, 4, and 6.

IV. CONCLUSION

We report high-resolution synchrotron x-ray scattering measurements of the intensity profiles in both longitudinal and transverse scans through a series of harmonics in the L_α phase of an oriented lyotropic lamellar liquid crystal supported by a solid.

Samples with thickness ~ 10–20 μm display algebraic peaks in accord with harmonic theory.[15,16] Measurement of the exponent x_n characterizing algebraic decay, and use of a prior measurement of the bulk splay elastic constant K, enables us to determine the bulk compressional elastic constant B. We find that for DLPC at 28°, $B = (1.9 \pm 1.0) \times 10^8$ ergs/cm^3. This represents the first measurement of the compressional elastic constant in this system. It is consistent in magnitude with that found in thermotropic Sm-A liquid crystals. The layer spacings obtainable by hydration of neutral phospholipids through the vapor phase are limited to water layers which are at most about half the thickness of the lipid bilayer. In this regime the effects of steric repulsion on the magnitude of B should not be significant.

Samples of thickness ~ 2 μm display longitudinal profiles which appear algebraic but are not consistent with harmonic theory. We speculate that in this thick-

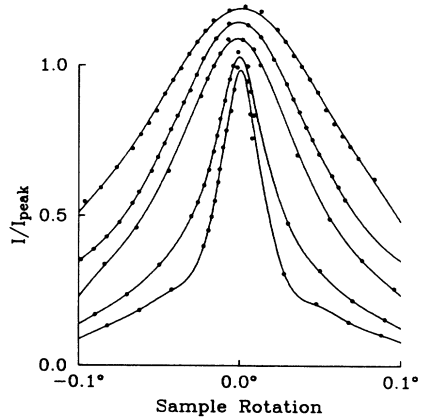

FIG. 12. Transverse intensity profiles at $Q_z = Q_n$ for harmonics $n = 1$, 2, 3, 4, and 6 of sample 3: normalized intensity vs sample rotation angle θ. Successive harmonics are displaced vertically for clarity. Solid lines are a guide to the eye. Measured FWHM of these scans are 40, 54, 98, 118, and 150 mdeg, respectively.

ness regime the fluctuation-quenching effects of the boundary conditions have significantly altered the fluctuation spectrum.

The consequences for longitudinal scans in the small Bragg angle regime of a nonuniform surface topography can be drastic. The Grandjean terrace configuration, energetically favored by the free surface of a Sm-*A* sample, illustrates these refractive effects quite dramatically.

ACKNOWLEDGMENTS

We acknowledge helpful discussions with P. Pershan and C. Safinya. We would like to thank members of the CHESS staff for their assistance. This work was supported by National Science Foundation Grant No. DMR-8404942, and benefited from the facilities of the Materials Science Center at Cornell University.

---

*Present address: GE Medical Systems, Milwaukee, WI 53201.

[1]L. Peliti and S. Leibler, Phys. Rev. Lett. **54**, 1690 (1985).
[2]R. Lipowsky and S. Leibler, Phys. Rev. Lett. **56**, 2541 (1986); S. Leibler and R. Lipowsky, Phys. Rev. B **35**, 7004 (1987).
[3]F. C. Larche, J. Appell, G. Porte, P. Bassereau, and J. Marignan, Phys. Rev. Lett. **56**, 1700 (1986).
[4]C. R. Safinya, D. Roux, G. S. Smith, S. K. Sinha, P. Dimon, N. A. Clark, and A. M. Belloq, Phys. Rev. Lett. **57**, 2718 (1986).
[5]G. S. Smith, C. R. Safinya, D. Roux, and N. A. Clark, Proceedings of the Eleventh International Liquid Crystal Conference, Berkeley, CA, 1986 (unpublished).
[6]D. Roux and C. R. Safinya, J. Phys. (Paris) **49**, 307 (1988).
[7]W. Helfrich, Z. Naturforsch. **28c**, 693 (1973).
[8]M. B. Schneider, J. T. Jenkins, and W. W. Webb, J. Phys. (Paris) **45**, 1457 (1984); Biophys. J. **45**, 891 (1984).
[9]F. Brochard and J. -F. Lennon, J. Phys. (Paris) **36**, 1035 (1975).
[10]P. G. de Gennes and C. Taupin, J. Phys. Chem. **86**, 2294 (1982).
[11]W. Helfrich, J. Phys. (Paris) **46**, 1263 (1985).
[12]S. A. Safran, D. Roux, M. E. Cates, and D. Andelman, Phys. Rev. Lett. **57**, 491 (1986).
[13]P. G. de Gennes, *The Physics of Liquid Crystals* (Clarendon, Oxford, 1974).
[14]R. E. Peierls, Proc. Cambridge Philos. Soc. **32**, 477 (1934); L. D. Landau, Phys. Z. Sowjetunion **11**, 26 (1937); N. D. Mermin and H. Wagner, Phys. Rev. Lett. **17**, 1133 (1966).
[15]L. Gunther, Phys. Lett. **25A**, 649 (1967); **26A**, 216(E) (1968); Y. Imry, Ann. Phys. (N.Y.) **51**, 1 (1969).
[16]A. Caille, C. R. Acad. Sci. **274B**, 891 (1972).
[17]J. Als-Nielsen, J. D. Litster, R. J. Birgeneau, M. Kaplan, C. R. Safinya, A. Lindegaard-Andersen, and S. Mathiesen, Phys. Rev. B **22**, 312 (1980)
[18]L. Gunther, Y. Imry, and J. Lajzerowicz, Phys. Rev. A **22**, 1733 (1980).
[19]P. Dutta and S. K. Sinha, Phys. Rev. Lett. **47**, 50 (1981).
[20]T. J. McIntosh, Biochim. Biophys. Acta **513**, 43 (1978).
[21]W. Helfrich, Z. Naturforsch. **33a**, 305 (1977).
[22]M. E. Fisher and D. S. Fisher, Phys. Rev. B **25**, 3192 (1982).
[23]S. G. J. Mochrie, A. R. Kortan, R. J. Birgeneau, and P. M. Horn, Phys. Rev. Lett. **53**, 985 (1984); Z. Phys. B **61**, 79 (1985).
[24]E. E. Gruber and W. W. Mullins, J. Phys. Chem. Solids **28**, 875 (1967).
[25]P. G. de Gennes, J. Chem. Phys. **48**, 2257 (1968).
[26]R. M. Servuss, W. Harbich, and W. Helfrich, Biochim. Biophys. Acta **436**, 900 (1976).
[27]J. -M. di Meglio, M. Dvolaitzky, L. Leger, and C. Taupin, Phys. Rev. Lett. **54**, 1686 (1985).
[28]J. Prost, Adv. Phys. **33**, 1 (1984).
[29]J. -P. LePesant, L. Powers, and P. Pershan, Proc. Natl. Acad. Sci. (U.S.A.) **75**, 1792 (1978).
[30]J. P. Marcerou, J. C. Rouillon, and J. Prost, Mol. Cryst. Liq. Cryst. **102**, 211 (1984).
[31]Cyrus R. Safinya (private communication).
[32]D. E. Moncton and R. Pindak, Phys. Rev. Lett. **43**, 701 (1979).
[33]P. A. Huang, P. W. Stephens, R. J. Birgeneau, P. M. Horn, and D. E. Moncton, Phys. Rev. B **28**, 6416 (1983).
[34]J. Als-Nielsen, R. J. Birgeneau, M. Kaplan, J. D. Litster, and C. R. Safinya, Phys. Rev. Lett. **39**, 1668 (1977).
[35]U. Bonse and M. Hart, Appl. Phys. Lett. **7**, 238 (1965).
[36]Crystal generously supplied by Lonny Berman, Department of Applied Physics, Cornell.
[37]CHESS A3 station documentation 1983 (unpublished).
[38]B. W. Batterman, CHESS Technical Memo. No. 6, 1981 (unpublished).
[39]N. P. Franks and W. R. Lieb, J. Mol. Biol. **141**, 43 (1980).
[40]M. Seul, Phys. Rev. Lett. **60**, 1150 (1988).
[41]R. W. James, *The Optical Principles of the Diffraction of X-rays* (Bell, London, 1948).